Surface & Coatings Technology 288 (2016) 30–35

Contents lists available at ScienceDirect

Surface & Coatings Technology

journal homepage: www.elsevier.com/locate/surfcoat

Corrosion-fatigue properties of plasma-based low-energy nitrogen ion implanted AISI 304 L austenitic stainless steel in borate buffer solution

K.S. Wang, H.L. Che, M.K. Lei *

Surface Engineering Laboratory, School of Materials Science and Engineering, Dalian University of Technology, Dalian 116024, China

ARTICLE INFO

Article history:
Received 6 October 2015
Revised 1 December 2015
Accepted in revised form 7 January 2016
Available online 12 January 2016

Keywords:
Plasma-based low-energy ion implantation
High-nitrogen face-centered-cubic phase
Corrosion-fatigue
Austenitic stainless steel
Borate buffer solution

ABSTRACT

AISI 304 L austenitic stainless steel was modified by using the plasma-based low-energy nitrogen ion implantation (PBLEII) at a process temperature of 400 °C for a processing time of 4 h in order to improve the corrosion-fatigue resistance of the austenitic stainless steel. A single high-nitrogen face-centered-cubic phase (γ_N) layer with a maximal nitrogen concentration of about 25 at.% was formed on the nitrogen-modified austenitic stainless steel. Compared with the original austenitic stainless steel, the γ_N phase layer on the austenitic stainless steel possessed a significant improvement in corrosion resistance in the borate buffer solution with a pH value of 8.4. The corrosion-fatigue properties of the γ_N phase layer on the austenitic stainless steel were examined by the push–pull fatigue experiments with a ratio R of tensile and compression of −1 in the borate buffer solution. The γ_N phase layer has an increased corrosion-fatigue strength up to 230 MPa from 180 MPa of the original austenitic stainless steel with an apparent increase of about 28%. The corrosion-fatigue crack initiation in the γ_N phase layer was found as a controllable stage in the fracture process at the interface between the γ_N phase layer and the austenitic stainless steel matrix with the arc corrosion-fatigue source. Some tiny corrosion-fatigue striations were obtained on the corrosion-fracture surfaces of the γ_N phase layer. The high density of slip bands and dislocations in the γ_N phase layer was able to prevent the crack initiation and propagation, leading to improvement of the corrosion-fatigue properties in the borate buffer solution.

1. Introduction

In order to improve the combined properties in wear and corrosion resistance, and anti-fatigue properties of Fe–Cr–Ni austenitic stainless steels, a series of nitrogen-modified processes have been successfully used to form a modification layer composed of a single high nitrogen face-centered-cubic (f.c.c.) phase (γ_N) with a high nitrogen concentration up to about 35 at.% on the austenitic stainless steels [1–3]. In the recent years, some studies of the fatigue properties of the nitrogen-modified austenitic stainless steels were performed to explore the possibility of improvement in the fatigue life [3–6]. Menthe et al. [3] reported that the γ_N phase layer on the AISI 304 L austenitic stainless steel modified by the pulsed direct current plasma nitriding increased the fatigue life, which was raised by a factor of 10 at low stress level around 230 MPa. Allen et al. [4] reported that the low-temperature plasma nitriding of the AISI 316 austenitic stainless steel possessed the higher plain fatigue limit not only, but also the higher fretting-fatigue limit, compared with that of the original stainless steel. However, Raman et al. [5] found that the low-temperature plasma nitriding of the AISI 304 austenitic stainless steel at 420 °C exhibited the inferior plain fatigue and fretting fatigue lives. Stinville et al. [6] investigated the fatigue durability of the γ_N phase layer on the AISI 316 L austenitic stainless steel with a significant improvement of the fatigue life in the low cycle fatigue range. Moreover, the improved corrosion-fatigue properties of the gas carburized AISI 316 austenitic stainless steel at a low carburizing temperature below 773 K in 3 wt.% NaCl solution were reported [7]. It was approved that the γ_N phase layer on the austenitic stainless steels was successfully applied in various industrial fields, even in nuclear power system [8]. However, there were some inconsistency in the reported fatigue properties of γ_N phase layer [3–6], unlike the improved wear and corrosion resistance, whose mechanisms were well-understood.

For the Fe–Cr–Ni austenitic stainless steels applied in the nuclear power stations using pressurized water reactor, the corrosion-fatigue crack in borate solution is one of typical failure types, which is always initiated by destruction and dissolution of the passive film on the austenitic stainless steels [9,10]. Therefore, the improvement in corrosion resistance would be beneficial to the corrosion-fatigue properties. The surface morphology, composition and structure of the austenitic stainless steels determine their corrosion-fatigue behavior, and the understanding on this issue could help to solve the structural reliability design problem occurring in borate solution. The application of austenitic stainless steels with γ_N phase layers may play an important role in improving its reliability in the borate solution-rich environment, such as the pressurized water reactor. However, there is little report on the corrosion-fatigue properties of γ_N phase in the borate solutions [11,12]. The influential mechanisms of

* Corresponding author.
E-mail address: mklei@dlut.edu.cn (M.K. Lei).

http://dx.doi.org/10.1016/j.surfcoat.2016.01.010
0257-8972/

nitrogen on the corrosion-fatigue properties improved by surface modification were not fully understood [13,14].

In this article, the corrosion-fatigue behavior of the γ_N phase layer formed on the AISI 304 L austenitic stainless steel by the plasma-based low-energy ion implantation (PBLEII) was investigated by means of the push–pull fatigue experiments with a ratio R of tensile and compression of −1 in the borate buffer solution with a pH value of 8.4, in order to explore the beneficial effect of nitrogen and its improvement mechanism on the corrosion-fatigue properties of austenitic stainless steel in the borate solution, and further to expand their wide industrial application.

2. Experiments

AISI 304 L austenitic stainless steel was supplied in a rolled bar after a solution treatment of 1050 °C under the vacuum followed an oil-quenching. Such a heat treatment provided the material a homogeneous structure with an average grain size of about 70 μm and no precipitated phases in the austenitic matrix. The metallographic, microstructural and corrosive samples were prepared as a disk with 20 mm in diameter and 6 mm in thickness. The cylindrical fatigue samples were machined with a gauge section of 4 mm in diameter and 15 mm in length with two loading screws used to clamp. The residual stress samples were prepared as thin strips of $70 \times 3 \times 0.7$ mm^3. Surface of all samples was ground using fine silicon carbide papers and polished using the 1.5 μm diamond paste. Subsequently, the following nitrogen-modified processing and measurement testing were applied.

The γ_N phase layer was obtained on the AISI 304 L austenitic stainless steel by PBLEII, namely by plasma source ion nitriding at a process temperature of 400 °C for a processing time of 4 h. The PBLEII device using an electron cyclotron resonance (ECR) microwave source, which is described elsewhere [15], was pumped down to a base pressure of 1.5×10^{-3} Pa. The nitriding pressure was 5×10^{-2} Pa with the addition of pure nitrogen. A pulsed negative potential of −2 kV with a repetition rate of 10^2–10^3 Hz and a length of 50–500 μs was used to bias the stainless steel samples. An average nitrogen ion current density of 0.6 mA/cm^2 was selected for PBLEII at 400 °C resulting from ion bombardment and auxiliary heating, for 4 h.

The nitrogen-modified surface on the AISI 304 L austenitic stainless steel by PBLEII was delineated by etching with Marble's etchant from 6 mol/l HCl and 0.4 mol/l Cu_2SO_4 agents in deionized water. The layer thickness was directly observed using an optical microscopy. The concentration-depth profile was measured by a Shimadzu EPMA-1600 electron probe microanalyser (EPMA). The near surface structure was analyzed using a Shimadzu XRD-6000 X-ray diffractometer (XRD) with Cu$K\alpha$ radiation. The microstructural characteristics were investigated using a Tecnai G220 S-Twin transmission electron microscopes (TEM). The stresses were calculated using Stoney's formula upon the measured curvature of thin plate stainless steel samples of 0.7 mm thickness before and after PBLEII. The samples with varied depth of nitriding layer were prepared from layer-by-layer removal using electrolytic polishing in an aqueous solution from mixing H_3PO_4 and H_2SO_4 in deionized water. The potentiodynamic polarization measurement of the nitrogen-modified samples was carried out using an EG&G PAR model 2273 potentiostat/galvanostat interfaced with a computer. Borate buffer solution with a pH value of 8.4 was prepared from mixing H_3BO_3 and $Na_2B_4O_7 \cdot 10H_2O$ analytical grade agents in deionized water. A conventional three-electrode cell was used as working electrode with 1 cm^2 exposed surface area. The counter electrode was a platinum sheet and all potentials were reported with respect to a saturated calomel electrode (SCE). Tensile tests were performed using an MTS Landmark 370.25 universal testing machine according to the ASTM E8/E8M standard. Corrosion-fatigue tests were executed using a Shimadzu EFH-LM20K1-02 servohydraulic testing machine by a sine push–pull loading controlled with the same maximum load in tension and compression of load ratio R of −1 with a loading frequency of 45 Hz in the borate buffer solution, according to the ASTM E466 standard. An acrylic chamber was used in the corrosion-fatigue tests to allow the suitable attachment of the samples immersed in the borate buffer solution and the controlled aeration of the solution. S–N curves were achieved in the borate buffer solution with a pH value of 8.4 at room temperature.

3. Results

Fig. 1 shows the optical micrograph of the nitrogen-modified layer on the AISI 304 L austenitic stainless steel by PBLEII at a process temperature of 400 °C for a processing time of 4 h. The thickness, microstructure, and microhardness of the nitrogen-modified layer on the austenitic stainless steel are characterized by the microscopic observation, and the Vickers microhardness indentations with a load of 0.1 N. An unetched white layer with a thickness of about 12 μm was observed on the nitrogen-modified austenitic stainless steel due to excellent corrosion resistance to the Marble's etchant. The microstructure of the austenitic matrix is generated from slipping system. A limited difference in thickness of nitrogen-modified layer was due to the anisotropic diffusion coefficients of the f.c.c. crystal lattice caused by the large growth stresses in expanded austenite, i.e. the stress-affected diffusion [16,17]. The microhardness-depth profile of the nitrogen-modified layer on the austenitic stainless steel is shown in Fig. 2, corresponding to the Vickers indentations in depth in Fig. 1. The most left point in Fig. 2 is on the outer surface of the γ_N layer and therefore not seen in Fig. 1. The maximal Vickers microhardness of the nitrogen-modified layer on the austenitic stainless steel was about HV0.1 N 13 GPa. It can be seen that the nitrogen-modified layer on the austenitic stainless steel matrix suffered from an abrupt drop in microhardness at the layer/matrix interface. Fig. 3 demonstrated a peak value of about 25 at.% and a rapid decrease around 12 μm of nitrogen concentration, which is consistent with the layer thickness observed in Fig. 1. A typical nitrogen concentration-depth profile with a nearly flat concentration evolution from the outer surface followed by a relatively abrupt decrease was observed on the nitrided surface of AISI 304 L austenitic stainless steel. The specific nitrogen concentration-depth profile was attributed to the interaction of nitrogen interstitials in a nonuniform system of the nitrogen-modified layer [18]. The structure of the nitrogen-modified layer on the AISI 304 L austenitic stainless steel and the original austenitic stainless steel were detected by XRD, respectively, as shown in Fig. 4. The original austenitic stainless steel has a standard f.c.c. lattice from the parent austenitic matrix (γ). The diffraction peaks of the nitrogen-modified layer on the austenitic stainless steel presented a set of broad diffraction peaks that appeared on the low angle side of each austenite peak of the γ matrix of original austenitic stainless steel. The (220) expanded austenite peak missing is due to the grain rotation

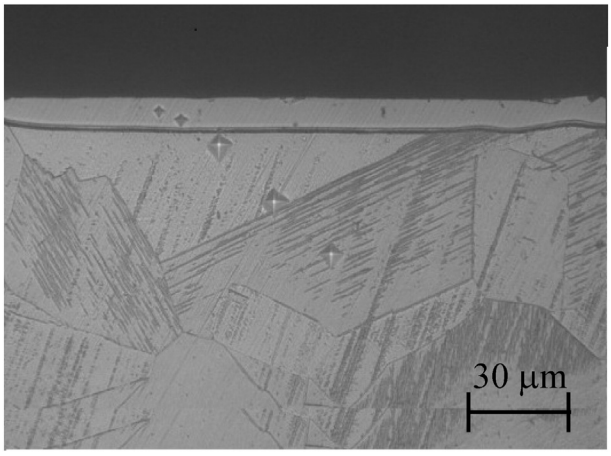

Fig. 1. Optical micrograph of the nitrogen-modified layer on the AISI 304 L austenitic stainless steel by PBLEII at a process temperature of 400 °C for a processing time of 4 h, together with the Vickers microhardness indentations by a load of 0.1 N.

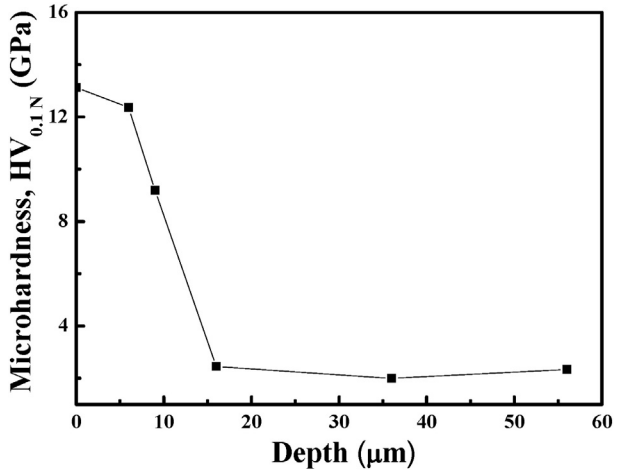

Fig. 2. Microhardness-depth profile of the γ_N phase layer on the AISI 304 L stainless steel by PBLEII at 400 °C for 4 h.

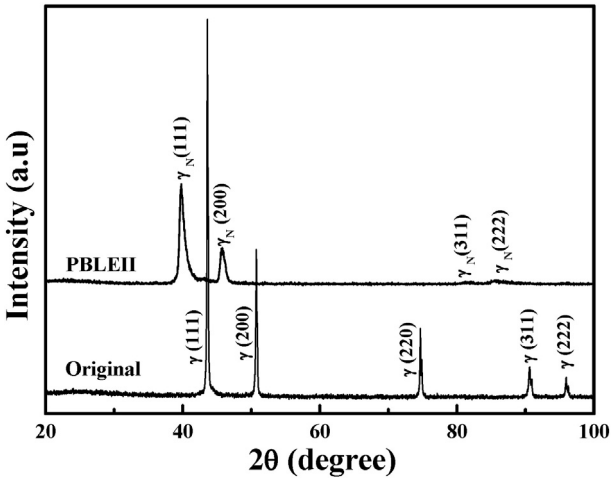

Fig. 4. XRD patterns of the nitrogen-modified layer on the AISI 304 L austenitic stainless steel by PBLEII at 400 °C for 4 h and the original austenitic stainless steel, respectively.

and the change in texture caused by the growth stress [19]. A single γ_N phase was confirmed unambiguously by the TEM observation with electron diffraction, as shown in Fig. 5. The high density of slip bands and dislocations was observed in the single γ_N phase layer on the nitrogen-modified austenitic stainless steel by PBLEII. It can be seen that the γ_N phase was formed on the nitrogen-modified AISI 304 L austenitic stainless steel by PBLEII, without any nitrides precipitation, such as chromium nitrides, γ'-Me_4N, ε-Me_{2-3} N and α' phases. The specific XRD pattern of the γ_N phase layer was a result of composition, stress and stacking faults [19–21].

Fig. 6 shows the measured residual stresses for the γ_N phase layer formed on the nitrogen-modified AISI 304 L austenitic stainless steel by PBLEII. It is found that compressive residual stresses can be resulted with maximal value of 800–1300 MPa dependent on the thickness of nitrogen-modified layers from about 5 to 14 μm. The thicker was the γ_N phase layer, the higher the compressive residual stress obtained in the surface. It should be emphasized that this method does not provide the actual residual stress profile over the expanded austenite layer, but must be an overall value.

Fig. 7 shows the potentiodynamic polarization curves in the borate buffer solution with a pH value of 8.4 for the γ_N phase layer formed on the nitrogen-modified AISI 304 L austenitic stainless steel by PBLEII and for the original austenitic stainless steel, respectively. The original austenitic stainless steel has a self-passivation feature without activation in the slightly alkaline solution [22,23]. The γ_N phase layer presented a strong tendency toward passivation with a decrease of the corrosion current density from (3–5) × 10^{-2} mA/cm^2 to (1–3) × 10^{-3} mA/cm^2, and a corresponding increase of the corrosion potential from −275 mV (SCE) to −231 mV (SCE). The critical potential of passivation decreased slightly from −22 mV (SCE) to −75 mV (SCE), and the critical current density of passivation was reduced by an order of magnitude, from 2.3 × 10^{-3} mA/cm^2 to 2.0 × 10^{-4} mA/cm^2. It can be seen that the γ_N phase layer on the austenitic stainless steel possessed a significant improvement in corrosion resistance in the borate buffer solution with a pH value of 8.4.

Fig. 8 shows the stress-strain curves in the borate buffer solution with a pH value of 8.4 for the nitrogen-modified AISI 304 L austenitic stainless steel samples with the γ_N phase layer by PBLEII and for the original austenitic stainless steel samples, respectively. The elongation and tensile strength of the original austenitic stainless steel samples in the borate buffer solution with a pH value of 8.4 were obtained as 108% and 729 MPa. Compared to the original austenitic stainless steel,

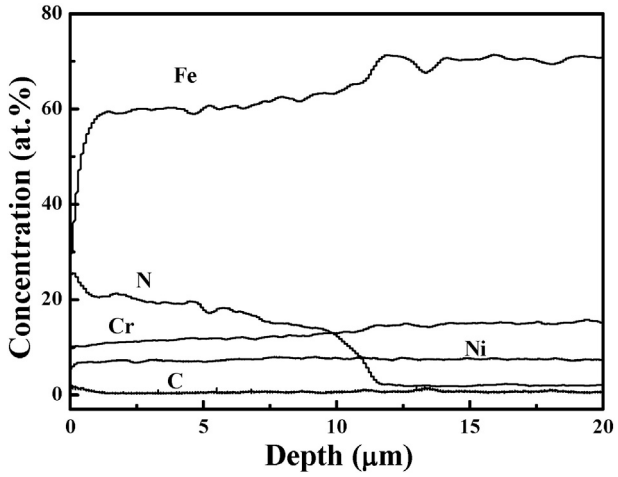

Fig. 3. Concentration-depth profiles by EPMA on the AISI 304 L austenitic stainless steel by PBLEII at 400 °C for 4 h.

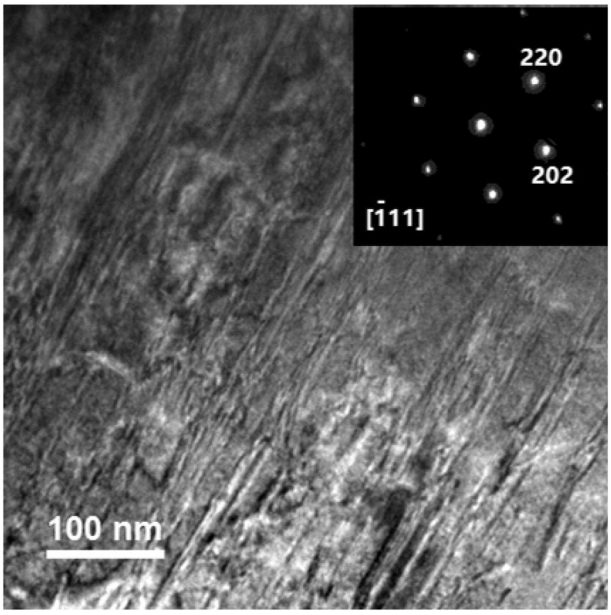

Fig. 5. TEM micrograph of γ_N phase layer formed on the AISI304L austenitic stainless steel by PBLEII at 400 °C for 4 h.

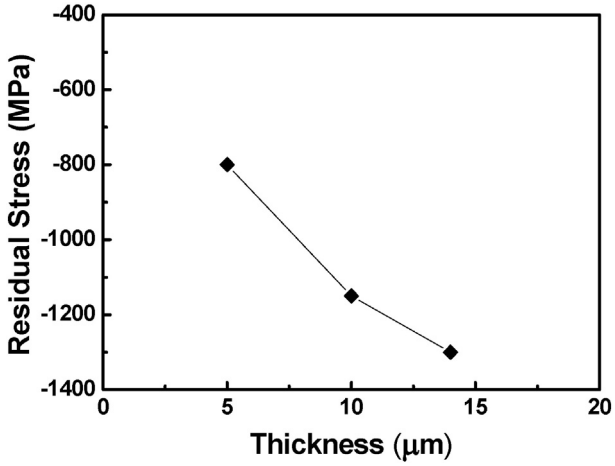

Fig. 6. The measured residual stresses for the γ_N phase layer formed on the AISI 304 L austenitic stainless steel by PBLEII at 400 °C for 4 h.

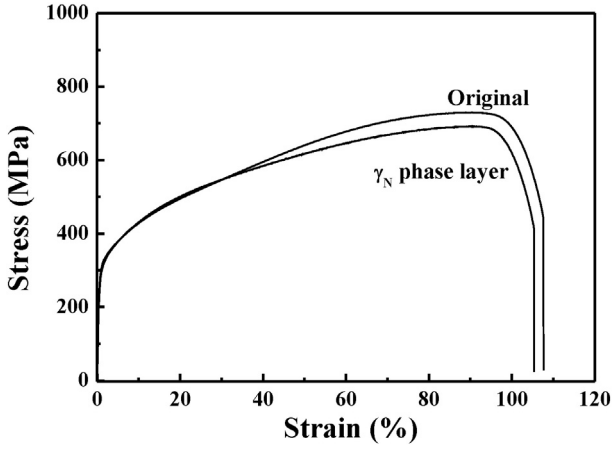

Fig. 8. Stress-strain curves in the borate buffer solution with a pH value of 8.4 for the nitrogen-modified AISI 304 L austenitic stainless steel samples with the γ_N phase layer by PBLEII and for the original austenitic stainless steel samples, respectively.

the nitrogen-modified austenitic stainless steel samples with the γ_N phase layer have a smaller elongation down to 105% and a slightly decreased tensile strength to 692 MPa, due to the stress concentrations around the crack formed on the γ_N phase layer [24]. The austenitic stainless steel with the γ_N phase layer presented a similar mechanical property in comparison with the original austenitic stainless steel.

Fig. 9 shows the S-N diagram in the borate buffer solution with a pH value of 8.4 for the nitrogen-modified AISI 304 L austenitic stainless steel samples with the γ_N phase layer by PBLEII and for the original austenitic stainless steel samples, respectively. The nitrogen-modified samples with a thickness of 12 μm have the optimized wear and corrosion resistance, and are adopted for corrosion-fatigue tests. The corrosion-fatigue life of the two-type samples is dependent on the level of the applied stress, as the applied stress falls until a definite corrosion-fatigue limit is reached, below which the corrosion-failure does not occur. The value of the corrosion-fatigue limit was arbitrarily chosen at 10^7 cycles for the samples which had not failed. In the borate buffer solution with a pH value of 8.4, the corrosion-fatigue strength of the original austenitic stainless steel was received as 180 MPa. The nitrogen-modified austenitic stainless steel with the γ_N phase layer possessed the improved corrosion-fatigue strength up to 230 MPa. The formation of the γ_N phase layer on the austenitic stainless steel resulted in a significant increase in the fatigue strength with the larger value of fatigue limit, compared with that of the original austenitic stainless steel.

Figs. 10 and 11 show the SEM images of the corrosion-fatigue fracture surface morphology in the borate buffer solution with a pH value of 8.4 for the original austenitic stainless steel samples and for the nitrogen-modified AISI 304 L austenitic stainless steel samples with the γ_N phase layer by PBLEII, respectively. The crack nucleation of the original austenitic stainless steel in the borate buffer solution with a pH value of 8.4 occurred at the outer surface of the samples, due to a cyclic slip deformation and the consequent formation of fatigue slip bands, as shown in Fig. 10. The crack initiation and the directions of crack propagation were indicated with the arrows. The crack propagation into the interior as radial lines from the corrosion-fatigue sources was observed for all the fractured samples. The fractured surface morphology of the original stainless steel was similar at all the applied stress conditions. Compared with the original austenitic stainless steel, the nitrogen-modified austenitic stainless steel with the γ_N phase layer changed the crack nucleation place which occurred at the layer/matrix interface, as shown in Fig. 11. The fatigue crack initiation with the γ_N phase layer was an arc interface line at the interface and therefore, no fish eyes crack initiation was found. With increasing the applied stress, the progress of the arc corrosion-fatigue sources showed along the different propagation routes. It was observed that the fatigue fibrous stripes which have been commonly observed in the fracture surface, were originated from the interface between the layer/matrix at an

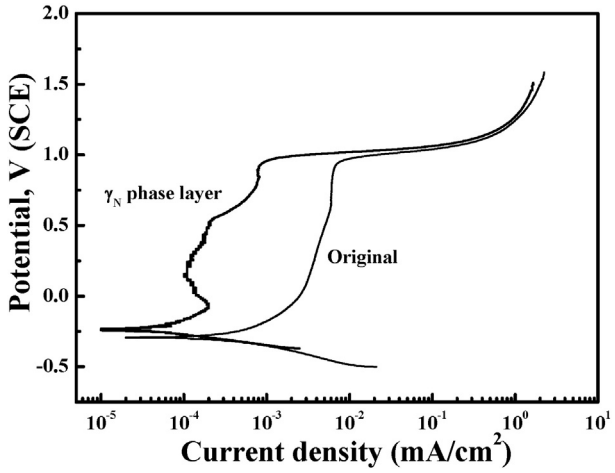

Fig. 7. Potentiodynamic polarization curves in the borate buffer solution with a pH value of 8.4 for the γ_N phase layer formed on the AISI 304 L austenitic stainless steel by PBLEII and for the original austenitic stainless steel, respectively.

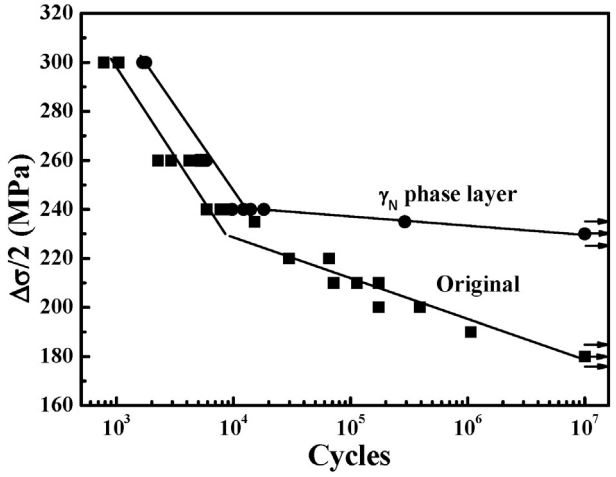

Fig. 9. S-N diagram in the borate buffer solution with a pH value of 8.4 for the nitrogen-modified AISI 304 L austenitic stainless steel samples with the γ_N phase layer by PBLEII and for the original austenitic stainless steel samples, respectively.

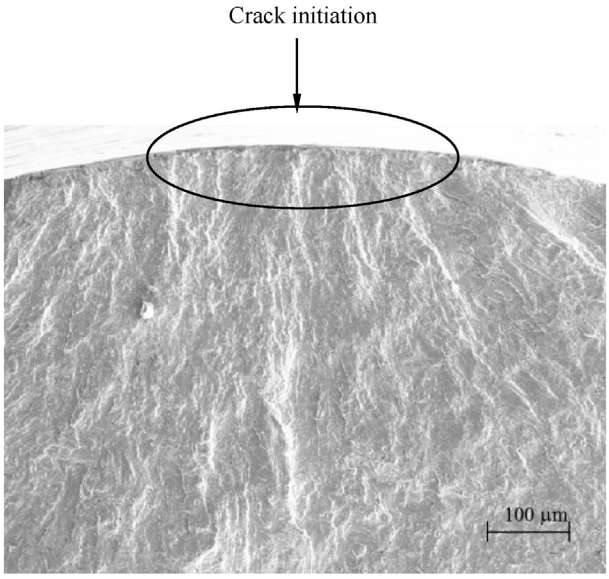

Fig. 10. SEM images of the corrosion-fatigue fracture surface morphology in the borate buffer solution with a pH value of 8.4 for the original AISI 304 austenitic stainless steel samples.

applied stress of 235 MPa (Fig. 11(a)). With an increased stress to 240 MPa, a few of the fatigue fibrous stripes can break outward through the interface (Fig. 11(b)). At the higher applied stress of 260 MPa, more fatigue fibrous stripes broke through the interface, but still not propagate to the outer surface of the nitrogen-modified austenitic stainless steel samples (Fig. 11(c)). Some tiny fatigue striations indicated in the inset with larger scale were found in the fracture surface of the γ_N phase layer. The striation spacing was about 0.3 μm (Fig. 11(d)). The γ_N phase layer displayed a typical fatigue fracture morphology with the fine fatigue striations.

4. Discussion

PBLEII onto the AISI 304 L austenitic stainless steel produced the single γ_N phase layer about 12 μm thick with a maximal nitrogen concentration of about 25 at.%. The γ_N phase layer on the nitrogen-modified austenitic stainless steel has a significant improvement in corrosion resistance in the borate buffer solution with a pH value of 8.4. The corrosion-fatigue properties of the γ_N phase layer on the austenitic stainless steel by the push–pull fatigue experiments with a ratio R of tensile and compression of −1 in the borate buffer solution have an increased corrosion-fatigue strength up to 230 MPa from 180 MPa of the original austenitic stainless steel with an apparent increase of about 28%.

The corrosion-fatigue source at the interface between the γ_N phase layer and the austenitic stainless steel matrix has an arc-shape instead of a fish-eye-like shape. The concentrated surface defects introduced by mechanical machining of the austenitic stainless steel samples were removed during the PBLEII process due to the ion bombardment, resulting in significant improvement in the surface integrity of the γ_N phase layer on the austenitic stainless steel. The similar arc fatigue source on the nitrogen-modified AISI 316 L austenitic stainless steel at 500 °C for 8 h was reported by the plasma nitriding [25], although the fish-eye-like fatigue source was by the several thermochemical treatment of the austenitic stainless steel [7,26,27]. The fatigue crack tends to initiate at the outer surface for the original austenitic stainless steel. After nitriding, the γ_N phase layer formed on the surface with a high compressive residual stress and an improved hardness suppressed the formation of fatigue crack source on the surface, which tends to initiate at the interface of the γ_N phase layer and the austenitic stainless steel matrix instead,

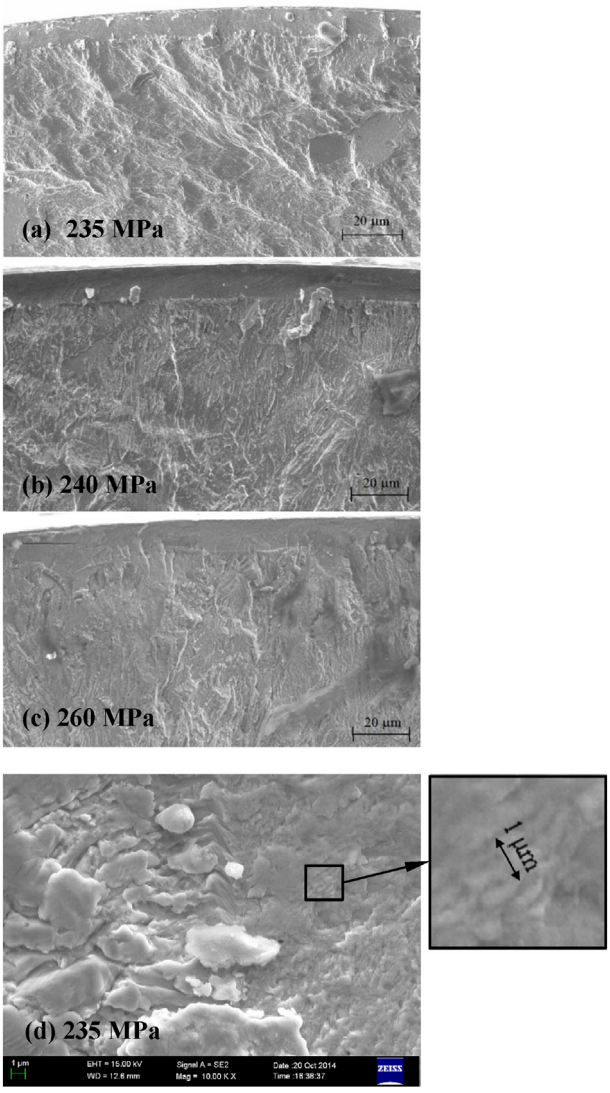

Fig. 11. SEM images of the corrosion-fatigue fracture surface morphology in the borate buffer solution with a pH value of 8.4 for the nitrogen-modified AISI 304 L austenitic stainless steel samples with the γ_N phase layer by PBLEII at 400 °C for 4 h.

as shown in Fig. 11. Moreover, for the corrosion-fatigue tests of Fe–Cr–Ni austenitic stainless steels in borate solution, the corrosion-fatigue cracking is always initiated by destruction and dissolution of the passive film on the austenitic stainless steels. Therefore, the improvement in corrosion resistance, as well as the increased hardness and compressive residual stress of γ_N phase layer would be beneficial to the corrosion-fatigue properties. The γ_N phase layer on the austenitic stainless steel has the high density of slip bands and dislocations caused by the super-saturated solution of the disordered nitrogen, leading to increase in the internal friction during the plastic deformation. Morton [28] proposed that the internal friction can be enhanced by the nitrogen diluted in the polycrystalline chromium. Wu and Nieh [29] suggested that the energy barrier for the nucleation process can be overcome by thermal fluctuation assisted by applied stresses and activation enthalpy was considered to be a measure of thermal barrier for an incipient plasticity. The value of activation enthalpy was calculated to be about 0.505 eV less than the activation energies for diffusion of interstitials, such as 1.05 eV for nitrogen atom. The increased internal friction restrained the crack initiation and further propagation in the γ_N phase layer. The stress concentration at the interface between the layer/matrix led to the crack initiation, however, the high compressive stress in the γ_N phase layer reduced the internal stress concentration, and the intact γ_N phase layer

could help to retard the crack propagation outward and increase the fatigue life.

The striations on the fracture surface are supposed to be remainders of the microplastic deformations at the crack tip. The striation spacing of the corrosion-fatigue in the γ_N phase layer was obtained as about 0.3 μm. Masuda et al. [30] summarized the relationship between striation spacing and fatigue crack propagation rate that are considered to be equal at the range of 1 μm/cycle > striation spacing > 0.1 μm/cycle. According to the crack propagated speed of 0.3 μm/cycle in the γ_N phase, the γ_N phase layer about 12 μm thick would be fractured in tens of cycle periods. However, the striations did not extend to the outer surface to form the cracks in the surface, due to increasing stress to high enough and quickly fracturing of the γ_N phase layer on the surface. The fracture of the γ_N phase layer took place at the late stage of crack propagation. Most of the corrosion-fatigue life of the γ_N phase layer formed on the austenitic stainless steel was attributed to the crack initiation stage in the high cycle fatigue under the lower stress condition, therefore, the more improvement in the corrosion-fatigue properties for the γ_N phase layer was found, compared with that in the low cycle fatigue under the higher stress condition. The fracture process in the γ_N phase layer formed on the austenitic stainless steel was described as four stages: crack initiation, crack propagation earlier stage, γ_N phase layer fracture, crack propagation later stage and ultimate fracture. The nitrogen supersaturated solution in the γ_N phase layer not only can block the crack initiated, but also inhibit the extension under the lower stress level. The difference in the fatigue life between the γ_N phase layer formed on the original austenitic stainless steel and the original stainless steel was understood as the applied stress decrease below 230 MPa (Fig. 8). After the γ_N phase layer fractured, the further fracture process was similar to that for the original austenitic stainless steel. However, if the applied stress was high enough, the γ_N phase layer could fracture at the first cycle and cannot prevent the crack initiation or the fatigue life decreased under the high stress condition [3].

The γ_N phase layer with a maximal nitrogen concentration of about 25 at.% on the austenitic stainless steel by PBLEII has the high density of slip bands and dislocations caused by the supersaturated solution of the disordered nitrogen. The high compressive stress in the γ_N phase layer inhibited the corrosion-fatigue crack initiation at the interface between the γ_N phase layer and the austenitic stainless steel matrix with the arc corrosion-fatigue source and prevented the crack propagation, leading to the improvement of the corrosion-fatigue properties in the borate buffer solution.

5. Conclusions

(1) AISI 304 L austenitic stainless steel was modified by using the PBLEII process at a process temperature of 400 °C for a processing time of 4 h. The corrosion-fatigue properties of the γ_N phase layer on the austenitic stainless steel were examined by the push–pull fatigue experiments with a ratio R of tensile and compression of −1 in the borate buffer solution with a pH value of 8.4.

(2) The γ_N phase layer has an increased corrosion-fatigue strength up to 230 MPa from 180 MPa of the original austenitic stainless steel with an apparent increase of about 28%. The corrosion-fatigue crack initiation for the γ_N phase layer on the austenitic stainless steel was originated at the interface between the γ_N phase layer and the austenitic stainless steel matrix with the arc corrosion-fatigue source.

(3) The small corrosion-fatigue striations were found in the corrosion-fracture surfaces of the γ_N phase layer. The high density of slip bands and dislocations in the γ_N phase layer was able to prevent the crack initiation and propagation, leading to the improvement of the corrosion-fatigue properties in the borate buffer solution.

Acknowledgments

The authors are very grateful to Professor J. Zhao, Dr. C.Q. Chen and Mr. B.C. Zheng for their contributory discussions and technical assistance. This work is supported by National Science Foundation of China under Grants No. 51271048 and 51321004.

References

[1] T. Bell, Key Eng. Mater. 373–374 (2008) 289.
[2] M.K. Lei, Z.L. Zhang, T.C. Ma, Surf. Coat. Technol. 131 (2000) 317.
[3] E. Menthe, A. Bulak, J. Olfe, A. Zimmermann, K.-T. Rie, Surf. Coat. Technol. 133–134 (2000) 259.
[4] C. Allen, C.X. Li, T. Bell, Y. Sun, Wear 254 (2003) 1106.
[5] S.G.S. Raman, M. Jayaprakash, Surf. Coat. Technol. 201 (2007) 5906.
[6] J.C. Stinville, P. Villechaise, C. Templier, J.P. Riviere, M. Drouet, Surf. Coat. Technol. 204 (2010) 1947.
[7] K. Tokaji, K. Kohyama, M. Akita, Int. J. Fatigue 26 (2004) 543.
[8] T. Bell, Surf. Eng. 18 (2002) 415.
[9] M. Vankeerberghen, G. Weyns, S. Gavrilov, B. Martens, J. Deconinck, J. Nucl. Mater. 384 (2009) 274.
[10] J. Xiao, S.Y. Qiu, Y. Chen, Z.X. Lin, Q. Xu, H.Y. Xie, Int. J. Fatigue 74 (2015) 65.
[11] P.M. Scott, Corrosion 56 (2000) 771.
[12] J. Arunkumar, C. David, C.V. Anto, K.G.M. Nair, S. Kalavathi, R. Rajaraman, G. Amarendra, B.K. Panigrahi, P. Magudapathy, J. Kennedy, J. Nucl. Mater. 414 (2011) 382.
[13] J.M. Cowling, J.W. Martin, Met. Technol. 8 (1981) 289.
[14] T.F. Azevedo, C.E.C.D. Andrade, S.V.D. Santos, A.S. Silva, S. Griza, Mater. Des. 85 (2015) 607.
[15] M.K. Lei, Z.L. Zhang, J. Vac. Sci. Technol. A 13 (1995) 2986.
[16] A. Martinavicius, G. Abrasonis, W. Moller, J. Appl. Phys. 110 (2011) 074907.
[17] D. Wu, H. Kahn, J.C. Dalton, G.M. Michal, F. Ernst, A.H. Heuer, Acta Mater. 79 (2014) 339–350.
[18] B.C. Zheng, K.S. Wang, Z.P. Zhang, H.L. Che, M.K. Lei, J. Vac. Sci. Technol. A 33 (2015) 021311.
[19] C. Templier, J.C. Stinville, P. Villechaise, P.O. Renault, G. Abrasonis, J.P. Rivière, A. Martinavičius, M. Drouet, Surf. Coat. Technol. 204 (2010) 2551.
[20] M.K. Lei, J. Liang, Surf. Eng. 26 (2010) 305.
[21] T.L. Christiansen, T.S. Hummelshoj, M.A.J. Somers, Surf. Eng. 26 (2010) 242.
[22] J.L. Lv, H.Y. Luo, Mater. Sci. Eng. C 34 (2014) 484.
[23] K.S. Wang, S. Tong, M.K. Lei, J. Electrochem. Soc. (2015) http://dx.doi.org/10.1149/2.0971510jes.
[24] J.C. Stinville, J. Cormier, C. Templier, P. Villechaise, Mater. Sci. Eng. A 605 (2014) 51.
[25] F. Yildiz, A.F. Yetim, A. Alsaran, A. Celik, I. Kaymaz, Tribol. Int. 44 (2011) 1979.
[26] N. Limodin, Y. Verreman, Mater. Sci. Eng. A 435–436 (2006) 460.
[27] S.M. Soleimani, A.R. Mashreghi, S.S. Ghasemi, M. Moshrefifar, Mater. Des. 35 (2012) 87.
[28] M.E.D. Morton, J. Appl. Phys. 33 (1962) 2768.
[29] D. Wu, T.G. Nieh, Mater. Sci. Eng. A 609 (2014) 110.
[30] C. Masuda, A. Ohta, S. Nishijima, E. Sasaki, J. Mater. Sci. 15 (1980) 1663.